RESEARCH ARTICLE

Key Points:
- Correlated electric field and downward current density seen in Cluster data
- The signature is reproduced in a model of magnetosphere-ionosphere coupling
- It implies an ionospheric cavity embedded in a larger-scale current system

Correspondence to:
A. J. B. Russell,
arussell@maths.dundee.ac.uk

Magnetospheric signatures of ionospheric density cavities observed by Cluster

A. J. B. Russell[1], T. Karlsson[2], and A. N. Wright[3]

[1]Division of Mathematics, University of Dundee, Dundee, UK, [2]Space and Plasma Physics, School of Electrical Engineering, KTH Royal Institute of Technology, Stockholm, Sweden, [3]Mathematical Institute, University of St. Andrews, St. Andrews, UK

Abstract We present Cluster measurements of large amplitude electric fields correlated with intense downward field-aligned currents, observed during a nightside crossing of the auroral zone. The data are reproduced by a simple model of magnetosphere-ionosphere coupling which, under different conditions, can also produce a divergent electric field signature in the downward current region, or correlation between the electric and perturbed magnetic fields. We conclude that strong electric field associated with intense downward field-aligned current, such as this observation, is a signature of ionospheric plasma depletion caused by the downward current. It is also shown that the electric field in the downward current region correlates with downward current density if a background field is present, e.g., due to magnetospheric convection.

1. Introduction

The coupling of the magnetosphere and ionosphere is mediated, in large part, through a global current circuit that links the two regions via field-aligned currents. The role of the ionosphere is often represented simply as a boundary condition through height-integrated conductivities with fixed values, which can be a good approximation when current systems do not significantly alter the conductivities. The focus of this paper is to demonstrate that in other circumstances the ionospheric conductivity can be dramatically altered and lead to a modification of the global current circuit as well as the magnetospheric electric and magnetic fields that carry these currents. This is most likely to occur on the nightside where ionosphere plasma density and conductivities are relatively low.

Doe et al. [1993] reported observations of *F* region density cavities at the base of downward field-aligned currents. These cavities were adjacent to *E* region aurora (at the base of upward field-aligned currents) suggesting the complete system comprised a pair of field-aligned currents closing in the ionosphere via a Pedersen current. They interpreted the cavity as being formed by ionospheric electrons being removed to supply the downward current. The observations presented by *Aikio et al.* [2004] support a similar picture to that of *Doe et al.* [1993], but the cavity was seen to form in the *E* region. *Aikio et al.* [2004] also noted that the depleted cavity was associated with an enhanced electric field, which *Aikio et al.* [1993] and later *Blixt and Brekke* [1996] suggested was necessary to drive the required Pedersen current through the region of reduced conductivity. Ionospheric plasma heating from this electric field can affect recombination rates, which can reduce the ionospheric plasma density further [*Zettergren and Semeter*, 2012].

Modeling of magnetosphere-ionosphere (MI) coupling relevant to the above observations has been performed by several authors [e.g., *Doe et al.*, 1995; *Blixt and Brekke*, 1996; *Karlsson et al.*, 2005; *Zettergren and Semeter*, 2012]. These studies generally represent the magnetosphere as a prescribed current or voltage source to drive the ionosphere, meaning that the magetospheric solution cannot evolve as a result of the development of the ionospheric cavity. However, these studies demonstrate convincingly that ionospheric cavities can be produced by supplying downward field-aligned currents.

Observations of a strong downward current channel situated between two auroral arcs have been studied by *Michell et al.* [2008] who identified it as a black stripe in optical data. They observed the width of the stripe to increase in time, suggesting that the width of the downward current sheet mapping out into the magnetosphere should also broaden. Cluster data analyzed by both *Marklund et al.* [2001] and *Aikio et al.* [2004] indicate that the magnetospheric downward current sheet can indeed broaden with time for strong currents and is consistent with ionospheric cavity formation. Hence, it is desirable to relax the assumption

that the magnetosphere can be represented as a fixed voltage or current source and adopt a more dynamic magnetospheric solution in response to the evolving ionosphere.

Attempts to model MI coupling in such a way that the magnetosphere can respond to changes in ionospheric conductivity have been developed by adopting an Alfvén wave model. *Streltsov and Lotko* [2004], *Cran-McGreehin et al.* [2007], and *Russell et al.* [2010] represent the magnetospheric current via a sum of two Alfvén waves: One from the magnetosphere that is incident upon the ionosphere, and one that is reflected from the ionosphere back to the magnetosphere. The reflected wave is affected by the presence of an ionospheric density cavity and so allows for a total magnetospheric current that is determined self-consistently with the ionospheric conductivity. These models all assume a sheet ionosphere represented through height-integrated conductivities and are able to demonstrate the nonlinear evolution of the coupled system to form density cavities and also to broaden in width for strong downward currents, as seen in the data. The formation of small scales can mean that electron inertial effects are important in the reflected wave [*Russell et al.*, 2013], causing the magnetospheric downward current to exhibit a filamentary structure which can be mapped from low-altitude satellites (FAST) to higher altitudes (Cluster) [*Wright et al.*, 2008]. Recently, the Alfvén wave model has been reformulated as a boundary condition that can be used in models which resolve the vertical structure of the ionosphere but have traditionally used a current or voltage source boundary condition [*Wright and Russell*, 2014].

Satellite observations of magnetospheric perpendicular electric and magnetic fields associated with large-scale field-aligned currents generally satisfy the relation

$$\Delta B/(\mu_0 \Delta E) = \Sigma_P, \tag{1}$$

where Σ_P is the height-integrated Pedersen conductivity and ΔB and ΔE are mutually perpendicular. In situations where Σ_P is fairly uniform, this leads to a strong correlation between ΔB and ΔE [e.g., *Ishii et al.*, 1992]. However, in a downward current channel with a cavity, we can expect low Σ_P leading to an enhanced electric field [*Streltsov and Marklund*, 2006]. From the wave viewpoint the enhanced electric field is associated with the reflection of an Alfvén wave off a low-conductivity cavity (reflection from an insulator doubles the incident electric field).

Streltsov and Marklund [2006] showed how an isolated up-down upward current system with a downward current cavity could be used to explain localized divergent electric fields sitting in the center of the downward current channel. In the present paper we present a new correlation seen in satellite data between the downward current density and the perpendicular electric field. Observations are summarized in section 2; section 3 presents a simple Alfvén wave model; section 4 presents simulation results and explains how the unusual correlation can be produced and what this tells us about the magnetosphere and ionosphere. Finally, section 5 summarizes our main results.

2. Observations

We present here data from the Electric Fields and Waves (EFW) instrument [*Gustafsson et al.*, 1997] and Fluxgate Magnetometer (FGM) [*Balogh et al.*, 2001] instruments on the four Cluster spacecraft. The Cluster spacecraft were launched in 2000 in a polar orbit with an apogee of 19.8 R_E and a perigee of 4.0 R_E, in geocentric distance. The data are available from the Cluster Science Archive.

Figure 1 shows data from an auroral zone crossing in the Northern Hemisphere on 25 December 2003. Ephemeris data are given in the figure, taking C3 as the reference spacecraft. The four panels show the Z component of the residual magnetic field ($\Delta B_{Z,MEE}$) and the Y component of the electric field ($E_{Y,MEE}$) for the four Cluster spacecraft C1–C4, with the electric field indicated by the blue curve, and the magnetic field by the red one. The coordinate system used is the magnetic-field-model, east, equatorward (MEE) system, where the X component is along a model geomagnetic field, Y is directed toward magnetic east, and Z is directed equatorward. The residual magnetic field is obtained by subtracting a background magnetic field determined by smoothing the original measurement with a sliding window with a width of 400 s. The satellite separation at this time was of the order of 200 km.

It is clear from Figure 1 that there is a substantial correlation between these two mutually orthogonal components of the electric and magnetic fields over the whole auroral zone crossing and for all four spacecraft.
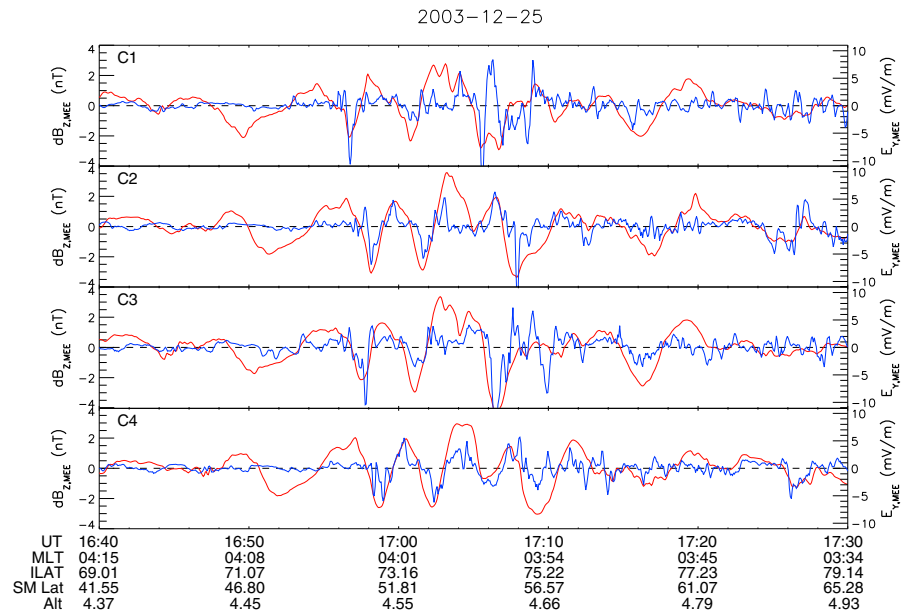
Figure 1. Electric and magnetic field data from Cluster for an auroral zone crossing on 25 December 2003 (C1 to C4 shown from top to bottom, respectively). Substantial correlation between $B_{Z,MEE}$ (red) and $E_{Y,MEE}$ (blue) at large scales is readily apparent. Ephemeris data are for C3.

Although this correlation breaks down on the smallest scales, and at some localized regions, we regard it as a clear indication of ionospheric conditions associated with a relative uniform conductivity.

In Figure 2 data are shown from another auroral zone crossing, in a similar format, although this time we show both perpendicular components of the electric and magnetic fields. The auroral crossing took place on 18 February 2004.

The main feature of the data is the crossing of three sheets of field-aligned current, first, a relatively smooth sheet of upward current approximately 800 km wide, a thinner sheet of downward current ($\approx$250 km), and finally, a wider sheet of predominantly upward currents ($\sim$1000 km wide). This current system is oriented with $\Delta\mathbf{B}$ in the east-west direction, and it remains essentially stationary in space for the whole 200 s period between the crossings of the central current sheet by C1 and C4. It is apparent that there is no similar correlation between E and B, as in Figure 1. Instead, there is a local enhancement of the electric field, associated with the region of positive slope of the residual magnetic field. This is true for all four spacecraft. If we use the infinite current sheet approximation to estimate the field-aligned current density we get the results shown in Figure 3, where the field-aligned current is shown in red, together with $E_{Z,MEE}$. Here we see that instead the electric field magnitude is very well correlated with the downward field-aligned current. The fact that the largest electric fields are seen in the region of downward current, and not in the regions of upward current, is clear indication that the magnetosphere-ionosphere interaction is very different in these two regions. In particular, we will discuss the difference in modification of ionospheric conductivities in these two regions.

3. Model

The modeling in this paper implements a two-way electrodynamic coupling between the magnetosphere and ionosphere, following the approach of *Cran-McGreehin et al.* [2007] and *Russell et al.* [2010]. For simplicity of illustration, we consider a one-dimensional system, which is sufficient to produce the effects of interest. The coordinate system used for the modeling sets z as vertically upward, y as poleward, and x as the remaining (east-west) coordinate. This is different to the MEE coordinate system used in section 2, but it maintains consistency with previous modeling work. The geomagnetic field close to the ionosphere is approximated as uniform and vertical with $\mathbf{B}_0 = B_0\hat{\mathbf{z}}$ ($B_0 < 0$ in the Northern Hemisphere) and invariance is assumed in the x direction.
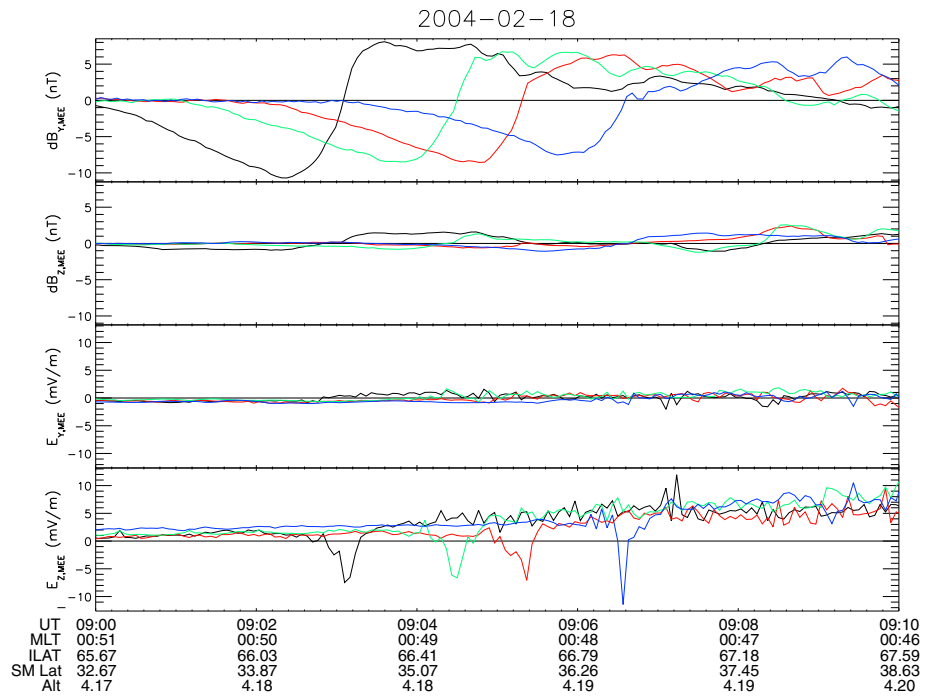
Figure 2. Electric and magnetic field data from Cluster for an auroral zone crossing on 18 February 2004. Black = C1, red = C2, green = C3, and blue = C4. Ephemeris data are for C3. The dominant feature is system of field-aligned current with magnetic perturbations oriented east-west and no correlation between *E* and *B*. Instead, *E* is enhanced in the region of positive slope of residual *B*.
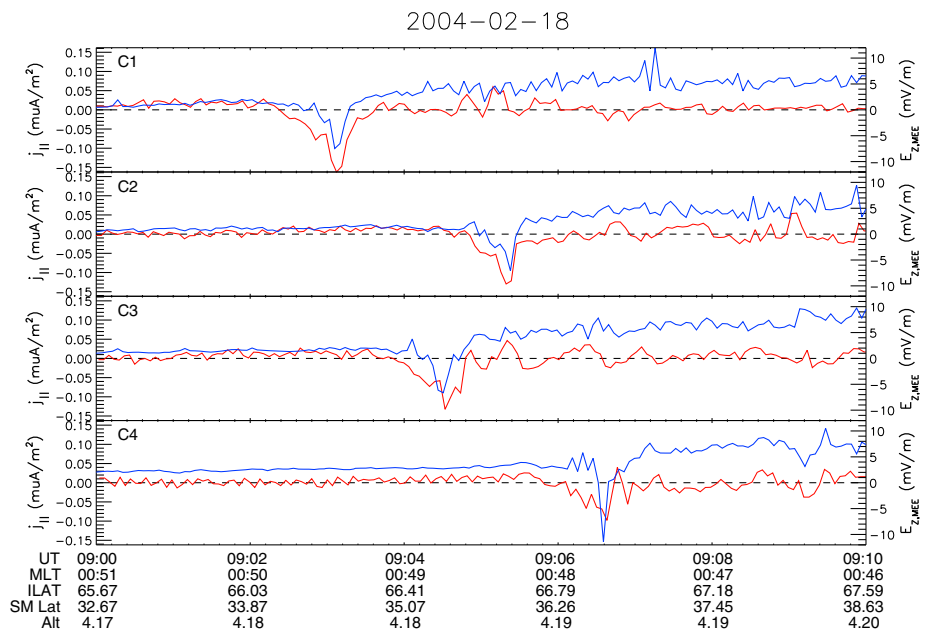

Figure 3. Perpendicular electric field from the 18 February 2004 auroral crossing (blue) and the field-aligned current obtained under the infinite current sheet approximation (red). These are very well correlated in the region of downward current. C1 to C4 are shown from top to bottom, respectively, and ephemeris data are for C3.

RUSSELL ET AL. 4

The magnetospheric part of the model is governed by ideal magnetohydrodynamics. Far from the iono-sphere, an electric field is generated that propagates downward as an incident Alfvén wave. The electric and magnetic field perturbations of this incident wave are $\mathbf{E}_i = E_i\hat{\mathbf{y}}$ and $\mathbf{b}_i = b_i\hat{\mathbf{x}}$, with

$$E_i = v_A b_i, \tag{2}$$

where $v_A = B/\sqrt{\mu_0\rho}$ is the Alfvén speed [*Walén*, 1944]. When the incident wave reaches the ionosphere it is partially reflected, thereby producing an upgoing wave with $\mathbf{E}_r = E_r\hat{\mathbf{y}}$, $\mathbf{b}_r = b_r\hat{\mathbf{x}}$, and

$$E_r = -v_A b_r. \tag{3}$$

The total electric and perpendicular magnetic fields are given by the sum of the incident and reflected wave fields, which at the MI interface is

$$\begin{aligned} E_y^T &= E_i + E_r = E_i(1 + r), \\ b_x^T &= b_i + b_r = b_i(1 - r), \end{aligned} \tag{4}$$

where $r = E_r/E_i$ defines the electric field reflection coefficient for the ionosphere and $b_r/b_i = -r$ follows from equations (2) and (3). Viewing the system in this way, the electric and magnetic fields in the magnetosphere are determined both by processes far out in the magnetosphere, which determine E_i, and also the state of the ionosphere, which determines the reflection coefficient r. The incident and reflected Alfvén wave fields are, in general, functions of y and t. For simplicity we assume that the incident fields are independent of time; however, the reflected field changes with time as electric currents (due to the waves) modify the ionospheric reflectivity. It is through this time dependence that we have a magnetospheric solution that actively responds to the state of the ionosphere.

The ionosphere is represented using a sheet ionosphere approximation. Throughout the ionosphere,

$$j_y = \frac{1}{\mu_0}\frac{\partial b_x}{\partial z} = \sigma_P E_y, \tag{5}$$

where σ_P is the Pedersen conductivity. The Hall conductivity does not appear in this formula because we have assumed invariance in the x direction and that all electric field in the ionosphere is associated with Alfvén waves; hence, $E_x = 0$. Integrating over the thickness of the ionosphere (z from 0 to h) and noting that $j_z|_{z=0} = 0 \Rightarrow b_x|_{z=0} = 0$ for a system of finite horizontal extent,

$$b_x|_{z=h} = \mu_0 \int_0^h \sigma_P E_y \, \mathrm{d}z = \mu_0 \Sigma_P E_y|_{z=h}. \tag{6}$$

Here Σ_P is the Pedersen conductance of the sheet ionosphere. When E_y maps well across the thickness of the ionosphere, equation (6) holds with $\Sigma_P = \int_0^h \sigma_P \, \mathrm{d}z$. This is usually a good approximation for horizontal length scales greater than 2 km. In situations where E_y is noticeably evanescent in the ionosphere, the same equation (6) holds with a modification to Σ_P that depends on the horizontal wavelength of the electric field [*Wright and Russell*, 2014; *Lysak*, 1991]. This paper considers horizontal scales $\gtrsim 10$km in the ionosphere, hence the large-scale (low-frequency) limit of Σ_P is appropriate and ionospheric reflectivity becomes independent of the incident wave.

Equation (6) acts as an ionospheric boundary condition for the magnetosphere and determines the ionospheric reflectivity. Combining it with equations (2)–(4),

$$r = \frac{1 - \Sigma_P/\Sigma_A}{1 + \Sigma_P/\Sigma_A}, \tag{7}$$

where $\Sigma_A = 1/(\mu_0 v_A)$ is the Alfvén conductance at the base of the magnetosphere. The ionosphere acts as a good conductor when $\Sigma_P \gg \Sigma_A$: in this case, the electric fields in the incident and reflected waves cancel to leave only a small residual total electric field, while the magnetic fields of the waves add together constructively. In the opposite limit, $\Sigma_P \ll \Sigma_A$, the ionosphere acts as an insulator: the electric fields of the waves add constructively and it is the magnetic fields that cancel. Variations of Σ_P/Σ_A over position and between events, and their impact on the magnetospheric fields, are central to the explanation we propose for the occurrence of different $j_{||}$-$E_\perp$ relationships.

The equations given in this section so far provide sufficient information to calculate E_y^T and b_x^T from known $E_i(y)$, Σ_A, and $\Sigma_P(y)$; however, self-consistency requires that the ionospheric response to E_y^T and b_x^T is also considered. Field-aligned currents in the magnetosphere are carried predominantly by the motion of electrons along the magnetic field. Thus, where upward (downward) magnetospheric currents meet the ionosphere, electrons will be added (removed) from the ionosphere, changing the electron density from its value in the absence of this additional source (sink). Equivalently, one may consider the Pedersen current that closes the current system in the ionosphere. This is carried by horizontal ion drifts in the direction of the electric field (made possible by ion-neutral collisions) that modify the ion density. Changes to electron and ion density occur in step, as required by quasi-neutrality, and they lead to temporal and spatial variations of Σ_P.

In the model, plasma density is followed using the electron continuity equation:

$$\frac{\partial n}{\partial t} = \frac{1}{e}\frac{\partial j_z}{\partial z} - \alpha(z)n^2 + s(z), \tag{8}$$

where n is the plasma number density, e the fundamental charge, j_z the vertical current density, $\alpha(z)$ the (height-dependent) recombination rate, and $s(z)$ a source term. The terms on the right-hand side represent, from left to right: addition (removal) of charge by electric currents, recombination, and production by a background ionization source, e.g., sunlight, starlight, or cosmic rays. Integrating equation (8) from $z=0$ to h and using $j_z|_{z=0}$, the height-integrated plasma density obeys

$$\frac{\partial N}{\partial t} = \frac{j_z|_{z=h}}{e} - \int_0^h \alpha n^2 \, \mathrm{d}z + S, \tag{9}$$

where S is the height-integrated production rate. In the sheet ionosphere approximation, the recombination term is assumed proportional to N^2 and can therefore be rewritten as SN^2/N_0^2, where N_0 is the steady state height-integrated plasma density when currents are absent. It is also informative to note that the magnitude of the strongest downward current that can be drawn from the ionosphere in a steady state is

$$j_c = eS, \tag{10}$$

which places a limit on steady state j_z, which is approached when downward current has evacuated the ionosphere and made recombination negligible. It follows that equation (9) becomes

$$\frac{\partial N}{\partial t} = \frac{j_z}{e} + \frac{j_c}{e}\left(1 - \frac{N^2}{N_0^2}\right). \tag{11}$$

The model is completed by assuming that Σ_P for the sheet ionosphere is proportional to N, i.e.,

$$\Sigma_P = \frac{\Sigma_{P0}}{N_0}N. \tag{12}$$

Summarizing, the impact of electric and magnetic fields on ionospheric reflectivity is encapsulated by equations (11), (12), and (7), while the effect of ionospheric reflectivity on the electric and magnetic fields is described by equation (4). This constitutes two-way electrodynamic feedback between the magnetosphere and ionosphere. In practice, the model system can be reduced to a single governing equation by combining equations (2), (4), (7), (9), and (12) with the z component of Ampère's law,

$$j_z = -\frac{1}{\mu_0}\frac{\partial b_x}{\partial y}, \tag{13}$$

to give

$$\frac{\partial N}{\partial t} = \frac{j_c}{e}\left(1 - \frac{N^2}{N_0^2}\right) - \frac{2\Sigma_{P0}}{e\mu_0\Sigma_A}\frac{\partial}{\partial y}\left(\frac{b_i(N/N_0)}{1 + (\Sigma_{P0}/\Sigma_A)(N/N_0)}\right). \tag{14}$$

For this paper, N is evolved numerically from an initial state, $N=N_0$, to a steady state for a specified b_i, by solving equation (14). Details of the numerical scheme are given by *Russell* [2010]. Once the steady state is obtained, E_y, j_z, and Σ_P (which are all consistent with one another) are readily evaluated and compared.
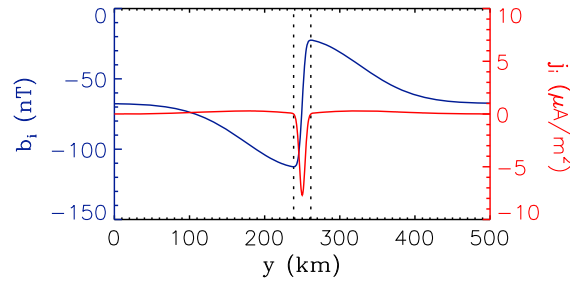
Figure 4. Magnetic field perturbation of the incident wave used to drive the simulation (blue) and the corresponding field-aligned current density, $j_i = (\partial b_i/\partial_y)/\mu_0$ (red). The driver is plotted for $b_{fac} = 45$ nT, $s = 75$ km, and $\alpha = 20$ in the presence of a background incident wave with $b_{bg}/b_{fac} = 1.5$. Dotted lines indicate the width of the downward current in the incident wave.

4. Results

Our main goal is to show how the correlated $E_\perp$-$j_{||}$ signature observed by Cluster (Figure 3) can result from self-consistent MI coupling. To do so, simulations were driven with an incident wave designed to produce a magnetic field similar to the observation (Figure 2, first panel), using a geometrical factor of 10 to approximately map observed length scales and field values to ionospheric altitude. The main feature is a field-aligned current system comprising a narrow region of downward current sandwiched between two much broader (hence much weaker) upward currents. A uniform background component was also permitted to include situations where the observed current system is embedded in a larger-scale system, such as one associated with a wider auroral arc or due to global convection. Given these requirements, the driver used was

$$b_i = b_{fac} \exp\left(-\frac{(y - y_0)^2}{2s^2}\right) \operatorname{erf}\left(\alpha \frac{(y - y_0)}{\sqrt{2}s}\right) + b_{bg},$$ (15)

and the simulated total magnetic field matched the mapped observation well for $b_{fac} = 45$ nT, $s = 75$ km, and $\alpha = 20$. Figure 4 plots b_i for these parameters and the corresponding current structure, $j_i = (\partial b_i/\partial_y)/\mu_0$. Note that the functional form of b_i corresponds to a simple pattern of two oppositely directed flows superimposed on the background convection.

The other important parameters are the conductance ratio Σ_{P0}/Σ_A, the strength of downward current density compared to the maximum that can be drawn from the ionosphere in a steady state, quantified as $2|j_i|/j_c$ where $\mu_0|j_i| = \min(-\partial b_i/\partial y)$, and the strength of the background incident wave compared to the amplitude of the incident wave associated with the field-aligned currents, b_{bg}/b_{fac}. These quantities were not constrained by the available observations, so they were varied within bounds appropriate to the time and location of the ionospheric foot point and typical large-scale auroral electric fields to determine a set of realistic values that reproduce the observation.

Figure 5 presents results from a simulation that produces the desired signature, showing a clear correlation between total $E_\perp$ and $j_{||}$ in the downward current region, of the type observed by Cluster (Figure 3). The
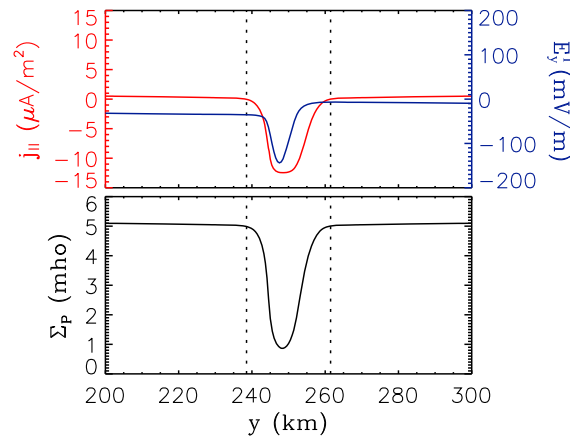

amplitudes of the normal electric field and current density also closely match the observed values mapped to the top of the ionosphere. The location of the correlation corresponds to a significant conductivity depletion in the ionosphere, produced by the downward current, and we suggest that magnetospheric measurements like those presented in Figures 2 and 3 should be interpreted as signatures of ionospheric density cavities.

The parameters used to obtain the correlated signature in Figure 5 were $\Sigma_A = 0.1$ mho, $\Sigma_{P0} = 5$ mho, $2|j_i|/j_c = 1.2$, and $b_{bg}/b_{fac} = 1.5$. Three considerations explain the success of these values and will be discussed momentarily. The discussion is aided if we notice that the steady state limit of (11) gives

$$N = N_0 \sqrt{1 - \frac{j_z}{j_c}},$$ (16)

Figure 5. Simulation results reproducing the observed correlation between $j_{||}$ and $E_\perp$. For this run, $\Sigma_{P0}/\Sigma_A = 50$, $2|j_i|/j_c = 1.2$, and $b_{bg}/b_{fac} = 1.5$. Dotted lines indicate the width of the downward current in the incident wave.
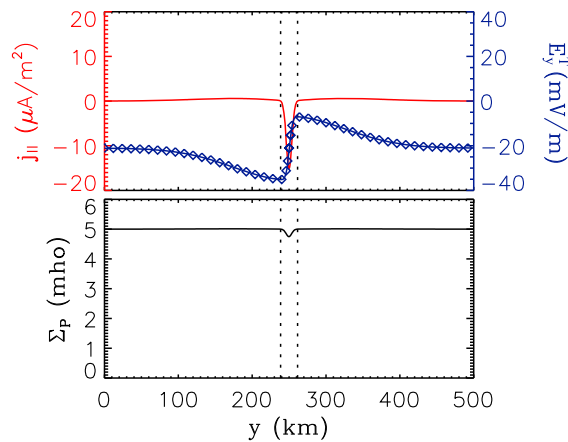
Figure 6. Simulation results showing correlation of perpendicular electric and magnetic fields. For this run, $\Sigma_{P0}/\Sigma_A = 50$, $2|j_i|/j_c = 0.1$, and $b_{bg}/b_{fac} = 0$. Diamonds show $b_\perp/(\mu_0\Sigma_{P0})$, which matches $E_\perp$ extremely well because of the small extent of the conductivity depletion.

which can be combined with equations (4) and (7), to obtain the steady state equation

$$E_y^T = \frac{2E_i}{1 + (\Sigma_{P0}/\Sigma_A)\sqrt{1 + j_z/j_c}}. \qquad (17)$$

The conductance ratio $\Sigma_{P0}/\Sigma_A = 50 \gg 1$ means that the ionosphere acts as a good conductor outside the downward current region. Hence, the incident and reflected electric fields cancel there, leaving a reasonably small value which is tens of mV in our simulation. This is confirmed by noting that equation (17) gives $E_y^T \ll 2E_i$ in upward or zero current regions for $\Sigma_{P0} \gg \Sigma_A$.

Having limited the electric field outside the downward current, correlation of $E_\perp$ and $j_{||}$ requires that the total electric field is large in the downward current compared to the modest values outside it. This is the role of the density cavity. If the downward current density is strong enough to deplete ionospheric density and create a cavity, then the ionosphere can locally become electrically insulating. In this location, incident and reflected waves do not cancel, so the perpendicular electric field can be much stronger than that seen outside the density cavity. For the simulation shown in Figure 5, $E_\perp$ in the downward current region reaches 140 mV/m in this way.

Reconciling this qualitative description with the steady state equations, equation (16) shows that the downward current density cannot exceed $-j_c$ in the steady state (otherwise N would become imaginary). Furthermore, a strong density cavity ($N \ll N_0$) corresponds to j_z approaching $-j_c$, which implies by equation (17) that E_y^T approaches its largest possible value of $2E_i$. This also helps to identify what constitutes strong downward current density. Seeking j_z in the steady state similar to $-j_c$ and noting that j_z is weaker than $2|j_i|$, the $j_{||}$-$E_\perp$ correlation is expected in simulations for which $2|j_i| > j_c$. (The ratio $2|j_i|/j_c$ has previously been shown to play an important role in determining the nature of the steady state [*Russell et al.*, 2010] and whether or not the downward current broadens [*Cran-McGreehin et al.*, 2007; *Russell et al.*, 2013]). Parameter studies confirm this: setting $2|j_i|/j_c \lesssim 1$ weakens both the depletion and the correlation. Indeed, for the limit $j_z \ll j_c$, ionospheric reflectivity remains reasonably uniform and the simulations readily produce the long-recognized $E_\perp \propto \delta B$ shown in the o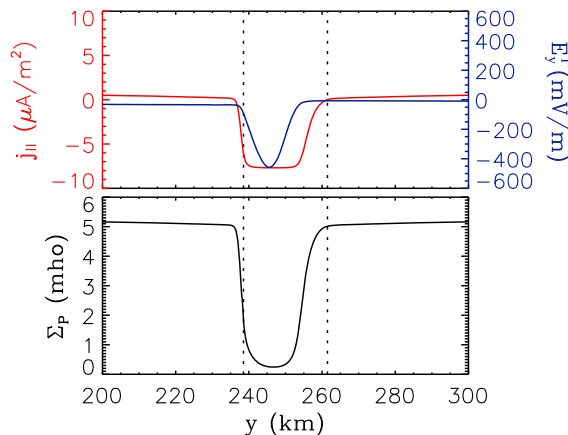bservation in Figure 1. A simulation example is presented in Figure 6, where $2|j_i|/j_c = 0.1$ leads to a steady state in which $b_\perp \approx \mu_0\Sigma_{P0}E_\perp$, consistent with the discussion in section 1.

There are also limits to how large $2|j_i|/j_c$ can be and still produce a clean $E_\perp$-$j_{||}$ correlation like the one observed by Cluster in Figure 3. This is because values $2|j_i|/j_c \gtrsim 2$ cause significant broadening of the downward current, which results in steady state profiles where $j_z \approx -j_c$ over a significant portion of the downward channel while E_y retains a peaked profile. This is demonstrated in Figure 7, which shows results from a simulation that has $2|j_i|/j_c = 2$ but otherwise is performed with driving and parameters identical to the one presented in Figure 5.

Figure 7. Simulation results showing an $E_\perp$-$j_{||}$ correlation that is distorted due to strong broadening of the downward current region and associated flattening of the downward current. For this run, $\Sigma_{P0}/\Sigma_A = 50$, $2|j_i|/j_c = 2.0$, and $b_{bg}/b_{fac} = 1.5$.

The last requirement is that E_i (equivalently b_i) should not change sign in the downward current region, otherwise E_y^T would change
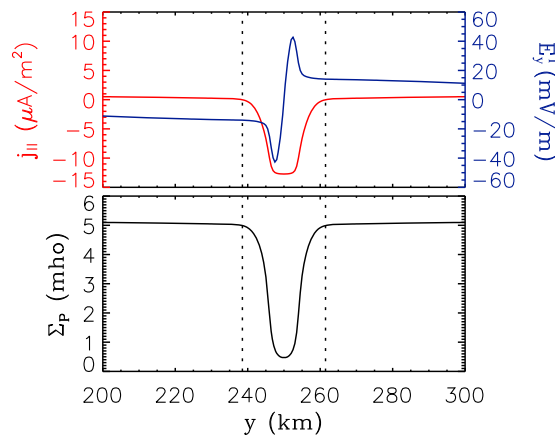
Figure 8. Simulation results showing a divergent electric field in the downward current region. For this run, $\Sigma_{P0}/\Sigma_A = 50$, $2|j_i|/j_c = 1.2$, and $b_{bg}/b_{fac} = 0$.

sign, breaking the observed correlation in Figure 3 (it is readily seen from equation (17) that $\text{sign}(E_y^T) = \text{sign}(E_i)$). For our model and driver, this condition requires a background electric field strong enough to ensure $E_{bg}/E_{fac} = b_{bg}/b_{fac} > 1$. Exploring this aspect further, Figure 8 presents results from a simulation with no background electric field, with driving and parameters otherwise identical to the simulation that produced the correlated $E_\perp\text{-}j_{||}$ signature shown in Figure 5. The electric field signature is again dominated by the strong field in the downward current region, but this time it has a divergent character and the electric field amplitude is considerably lower because of the electric field node. This limit recovers the signature analyzed in detail by *Streltsov and Marklund* [2006]. Like them, we find that this signature is associated with ionospheric density cavities. The distinction between this signature and the correlated $E_\perp\text{-}j_{||}$ signature (Figures 3 and 5) is the absence or presence of a background convection electric field.

5. Summary

This paper has presented an observation recorded by the Cluster satellites of a large amplitude electric field correlated with an intense downward field-aligned current and demonstrated that this signature is reproduced by a self-consistent model of magnetosphere-ionosphere coupling. From the modeling, it has been found that the conditions for a correlation between $E_\perp$ and $j_{||}$ in the downward current are ionospheric depletion leading to an ionospheric density cavity and presence of a larger-scale background electric field, e.g., due to magnetospheric convection.

The self-consistent MI coupling model we have employed is based on a dynamic wave picture in which the ionosphere is driven by an incident Alfvén wave generated by processes in the magnetosphere. The incident wave plus its reflection from the ionosphere provides the total wave fields that are observed in the magnetosphere. For example, a uniform convection of magnetospheric plasma over the ionosphere can be achieved by simply setting the incident Alfvén wave $b_i = b_{bg}$ in equation (15) where b_{bg} is a constant. Here we have neglected the field-aligned current system in equation (15) by simply setting $b_{fac} = 0$. There will also be a uniform background electric field in the incident Alfvén wave according to equation (2). If this Alfvén wave reflects off a uniform highly conducting ionosphere ($\Sigma_P/\Sigma_A > 1$), then the reflected wave acts to reduce the total E_y^T to a fraction of the incident value, while producing a total magnetic field $b_x^T \approx 2b_i$. The fact that there is a significant magnetic field at the base of the magnetosphere means there is Pedersen current associated with the background convection. However, because there is a highly conducting ionosphere, only a small electric field is required to drive it as indicated by Ohm's law and the small value of E_y^T. This is the self-consistent view of background magnetospheric convection from the Alfvén wave perspective.

Field-aligned currents and magnetosphere-ionosphere coupling are often described in terms of electrical current circuits and this provides a complementary interpretation. Figure 9 (left) shows a large-scale current system, where magnetospheric convection produces broad upward and downward field-aligned currents, which close as Pedersen current, J_P, in the ionosphere. Note that J_P is largest between the upward and downward current regions. The horizontal electric field needed to drive the Pedersen current, given uniform Σ_P, is also sketched in the figure. More realistically, the field-aligned currents add or remove electrons from the ionosphere and thereby modify the Pedersen conductivity, so Σ_P is slightly enhanced in upward current regions and decreased in downward current regions. However, for the relatively weak field-aligned current densities associated with a large-scale system, the effect of the modified conductivities on the electric field is not dramatic. If one looks locally at some small subregion near the center of the current system (i.e., near
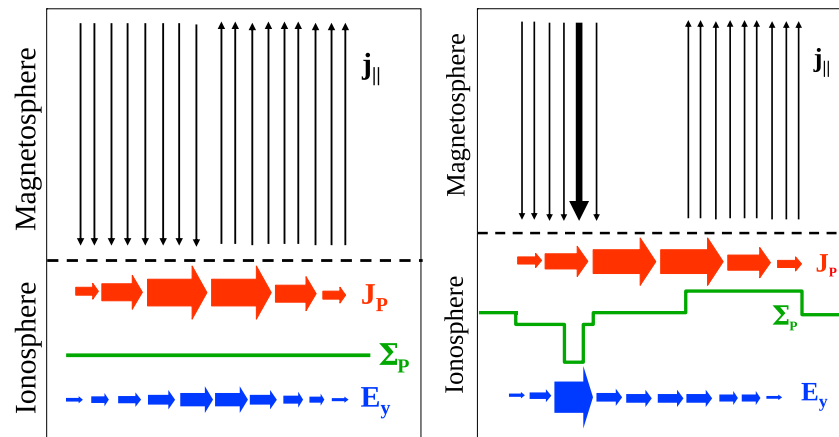
Figure 9. Current circuit cartoon of conditions giving the $E_\perp$-$j_\parallel$ observed by Cluster and reproduced in our model. (left) A large-scale current system in which broad upward and downward field-aligned currents close in the ionosphere as Pedersen current. (right) Adding an intense downward field-aligned current locally depletes the ionosphere and makes it more electrically insulating. In the cavity, a strong electric field is required to drive the Pedersen current associated with the large-scale background current system.

to where J_P is largest), then one finds significant background values of b_x and E_y which vary little over the scale of interest, consistent with the wave description of background convection outlined above.

If we now introduce a localized intense field-aligned current system by having $b_{fac} \neq 0$ in equation (15), how does the system adjust? The effect of the new field-aligned currents is twofold. First, they too must close via Pedersen current, although the contribution to J_P will be small if the total current in the small-scale system is small compared to the total current in the background system. Second, the intense field-aligned currents also modify the Pedersen conductivity, only this time the impact of an intense downward current density on Σ_P may be substantial, creating an ionospheric density cavity. From the wave viewpoint a density cavity will affect the reflection properties. In the highly conducting (upward current regions) the E_y^T will remain small. However, in the depleted downward current region Σ_P may drop making it a poor conductor. Here E_y^T will be enhanced due to the incident and reflected Alfvén wave fields being in phase. Importantly, we find that a large perpendicular E_y^T may occur where Σ_P is reduced, and this will occur in the downward current region. This is the novel correlation seen in Figure 3 that we set out to explain. This scenario is also sketched as a current circuit, in Figure 9 (right). If the small-scale downward current depletes Σ_P while the local Pedersen current is dominated by the large scale system, then Ohm's law will require an electric field $E_y = J_P/\Sigma_P$ that is locally enhanced to maintain current closure. This may be significantly larger than the E_y outside the depletion; hence, the correlated signature is recovered.

Of course, a fully self-consistent picture will need to recognize that a seriously evacuated ionosphere may struggle to carry any current, so the original current would need to close elsewhere. Such self-consistency is realized easily in the wave description as the maximum electric field that can be achieved is twice E_i. Hence, an upper limit for the Pedersen current is $J_P = 2E_i\Sigma_P$, and if the Pedersen current exceeds this then the system will adjust by reducing the downward current by having the b_r largely cancel b_i where the conductivity is low,and hence limit the downward field-aligned current density. Other behavior identified in the wave picture includes allowing the downward current region to broaden in space so that sufficient ionospheric electrons may be accessed to feed $j_\parallel$ [*Cran-McGreehin et al.*, 2007; *Russell et al.*, 2010].

If the Cluster data presented in Figures 2 and 3 is interpreted as the magnetospheric signature of magnetosphere-ionosphere coupling, as we suggest, then several inferences can be made about conditions during the event. First, the observed correlation between $E_\perp$ and $j_\parallel$ in the downward current region suggests that the small-scale current system was embedded in a much larger system, which provided a significant background Pedersen current in the ionosphere but is not readily apparent in the processed Cluster data. Were this not the case, then we would expect the electric field to have a bipolar signature in the downward current region, similar to that shown in Figure 8 and discussed previously by *Streltsov and Marklund* [2006], or a hybrid signature in the case of a low background Pedersen current. The Regions 1 and 2 Birkeland currents are a natural candidate for the background current system. Second, the cleanness of the signature

suggests that the ionosphere was acting as a good conductor outside the downward current region, with $\Sigma_P \gg \Sigma_A$ giving a small electric field there, while the downward current density was strong enough to significantly change the ionospheric reflectivity inside the corresponding density cavity.

The values and profiles of the downward current density also lead to some interesting remarks. The peak value of $j_\parallel$ measured by Cluster was between $0.16\,\mu Am^{-2}$ (C1) and $0.08\,\mu Am^{-2}$ (C4). Mapped geometrically to the ionosphere and neglecting attenuation along the field line, this suggests that ionization sources in the ionosphere were able to support downward currents of the order of 8 to $16\,\mu Am^{-2}$. Furthermore, C4 was the last spacecraft to pass through the downward current region, and it measured both the lowest peak current density and the strongest peak electric field. There is also some suggestion in Figure 3 that the current profile recorded by C4 is flatter than those recorded by the other spacecraft. This may suggest that the system was not in a steady state throughout the entire 200 s duration of the encounter, but rather that the density cavity was still evolving to its most depleted state, which the data from C4 indicates would be similar to the simulation steady state shown in Figure 7. Spatial separation between the tracks of the four spacecraft means some caution is needed in interpreting differences between the four spacecraft as time evolution. However, if this interpretation were used, then a critical current density of about $j_c \approx 8\,\mu Am^{-2}$ would be implied, with the initial downward current density comfortably exceeding this ($j_z \gtrsim 16\,\mu Am^{-2}$ implied by data from C1), i.e., ideal conditions for ionospheric depletion and current broadening [*Cran-McGreehin et al.*, 2007; *Russell et al.*, 2010, 2013].

Finally, our modeling has demonstrated that self-consistent MI coupling can produce strong electric fields in downward field-aligned currents, and the results appear to be consistent with the Cluster observations presented in section 2; however, proving conclusively that the ionosphere played an important role ultimately requires observations of the ionosphere at the magnetic foot point, which we do not have for the 18 February 2004 auroral crossing. The best case scenario would be to have conjugate data from incoherent scatter radar, which could confirm (or rule out) the presence of a density cavity in the downward current region. So far, we have been unable to find a similar event for which complementary observations are available, but we suggest that acquisition of such data could form the basis of a valuable future campaign. Additional evidence for an ionospheric role could also be obtained less directly by simultaneous observation of field-aligned currents in conjugate hemispheres, or from the statistical occurrence of events displaying $j_\parallel$-$E_\perp$ correlations or the bipolar signature discussed by *Streltsov and Marklund* [2006]. The intention would be to explore the relation between occurrence rate and ionospheric conditions since our modeling predicts that strong electric fields appear in the downward current more commonly when the ionosphere is more easily depleted.

References

Aikio, A., K. Mursula, S. Buchert, F. Forme, O. Amm, G. Marklund, M. Dunlop, D. Fontaine, A. Vaivads, and A. Fazakerley (2004), Temporal evolution of two auroral arcs as measured by the Cluster satellite and coordinated ground-based instruments, *Ann. Geophys.*, *22*, 4089–4101, doi:10.5194/angeo-22-4089-2004.

Aikio, A. T., H. J. Opgenoorth, M. A. L. Persson, and K. U. Kaila (1993), Ground-based measurements of an arc-associated electric field, *J. Atmos. Terr. Phys.*, *55*, 797–808.

Balogh, A., et al. (2001), The Cluster magnetic field investigation: Overview of in-flight performance and initial results, *Ann. Geophys.*, *19*, 1207–1217, doi:10.5194/angeo-19-1207-2001.

Blixt, E. M., and A. Brekke (1996), A model of currents and electric fields in a discrete auroral arc, *Geophys. Res. Lett.*, *23*, 2553–2556, doi:10.1029/96GL02378.

Cran-McGreehin, A. P., A. N. Wright, and A. W. Hood (2007), Ionospheric depletion in auroral downward currents, *J. Geophys. Res.*, *112*, A10309, doi:10.1029/2007JA012350.

Doe, R. A., M. Mendillo, J. F. Vickrey, L. J. Zanetti, and R. W. Eastes (1993), Observations of nightside auroral cavities, *J. Geophys. Res.*, *98*, 293–310, doi:10.1029/92JA02004.

Doe, R. A., J. F. Vickrey, and M. Mendillo (1995), Electrodynamic model for the formation of auroral ionospheric cavities, *J. Geophys. Res.*, *100*, 9683–9696, doi:10.1029/95JA00001.

Gustafsson, G., et al. (1997), The electric field and wave experiment for the Cluster mission, *Space Sci. Rev.*, *79*, 137–156, doi:10.1023/A:1004975108657.

Ishii, M., M. Sugiura, T. Iyemori, and J. A. Slavin (1992), Correlation between magnetic and electric field perturbations in the field-aligned current regions deduced from DE 2 observations, *J. Geophys. Res.*, *97*, 13,877–13,887, doi:10.1029/92JA00110.

Karlsson, T., G. Marklund, N. Brenning, and I. Axnas (2005), On enhanced Aurora and low-altitude parallel electric fields, *Phys. Scr.*, *72*, 419–422, doi:10.1238/Physica.Regular.072a00419.

Lysak, R. L. (1991), Feedback instability of the ionospheric resonant cavity, *J. Geophys. Res.*, *96*, 1553–1568, doi:10.1029/90JA02154.

Marklund, G. T., et al. (2001), Temporal evolution of the electric field accelerating electrons away from the auroral ionosphere, *Nature*, *414*, 724–727, doi:10.1038/414724a.

Michell, R. G., K. A. Lynch, and H. C. Stenbaek-Nielsen (2008), Ground-based observational signature of a downward current channel in an active auroral arc, *Geophys. Res. Lett.*, *35*, L08101, doi:10.1029/2008GL033596.

Russell, A. J. B. (2010), Coupling of the solar wind, magnetosphere and ionosphere by MHD waves, PhD thesis, Univ. of St Andrews, St Andrews, Fife, U. K.

Russell, A. J. B., A. N. Wright, and A. W. Hood (2010), Self-consistent ionospheric plasma density modifications by field-aligned currents: Steady state solutions, *J. Geophys. Res.*, *115*, A04216, doi:10.1029/2009JA014836.

Russell, A. J. B., A. N. Wright, and A. V. Streltsov (2013), Production of small-scale Alfvén waves by ionospheric depletion, nonlinear magnetosphere-ionosphere coupling and phase mixing, *J. Geophys. Res. Space Physics*, *118*, 1450–1460, doi:10.1002/jgra.50168.

Streltsov, A. V., and W. Lotko (2004), Multiscale electrodynamics of the ionosphere-magnetosphere system, *J. Geophys. Res.*, *109*, A09214, doi:10.1029/2004JA010457.

Streltsov, A. V., and G. T. Marklund (2006), Divergent electric fields in downward current channels, *J. Geophys. Res.*, *111*, A07204, doi:10.1029/2005JA011196.

Walén, C (1944), On the theory of sunspots, *Ark. Mat. Astron. Fys.*, *30*, 1–87.

Wright, A. N., and A. J. B. Russell (2014), Alfvén wave boundary condition for responsive magnetosphere-ionosphere coupling, *J. Geophys. Res. Space Physics*, *119*, 3996–4009, doi:10.1002/2014JA019763.

Wright, A. N., C. J. Owen, C. C. Chaston, and M. W. Dunlop (2008), Downward current electron beam observed by Cluster and FAST, *J. Geophys. Res.*, *113*, A06202, doi:10.1029/2007JA012643.

Zettergren, M., and J. Semeter (2012), Ionospheric plasma transport and loss in auroral downward current regions, *J. Geophys. Res.*, *117*, A06306, doi:10.1029/2012JA017637.